LETTER

doi:10.1038/nature24280

Single-cell RNA sequencing reveals a signature of sexual commitment in malaria parasites

Asaf Poran[1,2,3]*, Christopher Nötzel[4,5]*, Omar Aly[1,2], Nuria Mencia-Trinchant[6], Chantal T. Harris[5,7], Monica L. Guzman[6], Duane C. Hassane[1,6], Olivier Elemento[1,2] & Björn F. C. Kafsack[5]

Pathogens have to balance transmission with persistence. For *Plasmodium falciparum*, the most widespread and virulent malaria parasite, persistence within its human host requires continuous asexual replication within red blood cells, while its mosquito-borne transmission depends on intra-erythrocytic differentiation into non-replicating sexual stages called gametocytes[1]. Commitment to either fate is determined during the preceding cell cycle that begins with invasion by a single, asexually committed merozoite and ends, 48 hours later, with a schizont releasing newly formed merozoites, all committed to either continued asexual replication or differentiation into gametocytes[2,3]. Sexual commitment requires the transcriptional activation of *ap2-g* (PF3D7_1222600)[4,5], the master regulator of sexual development, from an epigenetically silenced state during asexual replication[6,7]. AP2-G expression during this 'commitment cycle' prepares gene expression in nascent merozoites to initiate sexual development through a hitherto unknown mechanism[2,4]. To maintain a persistent infection, the expression of *ap2-g* is limited to a sub-population of parasites (1–30%, depending on genetic background and growth conditions). As sexually committed schizonts comprise only a sub-population and are morphologically indistinguishable from their asexually committed counterparts, defining their characteristic gene expression has been difficult using traditional, bulk transcriptome profiling[8]. Here we use highly parallel, single-cell RNA sequencing[9] of malaria cultures undergoing sexual commitment to determine the transcriptional changes induced by AP2-G within this sub-population. By analysing more than 18,000 single parasite transcriptomes from a conditional AP2-G knockdown line and NF54 wild-type parasites at multiple stages of development, we show that sexually committed, AP2-G$^+$ mature schizonts specifically upregulate additional regulators of gene expression, including other AP2 transcription factors, histone-modifying enzymes, and regulators of nucleosome positioning. These epigenetic regulators may act to facilitate the expression and/or repression of genes that are necessary for the initiation of gametocyte development in the subsequent cell cycle.

To test whether we could reproducibly distinguish multiple parasite stages on the basis of single-cell RNA sequencing (RNA-seq), we first analysed a subset of 3,500 single-cell transcriptomes (SCTs) of individual parasites at several stages of intra-erythrocytic development (Fig. 1a, Extended Data Fig. 1 and Supplementary Table 1). The resulting SCTs readily segregated into distinct clusters by life-cycle stage as determined by the time of parasite collection, showing little apparent difference between technical or biological replicates (Fig. 1b, c), and with the number of individually captured transcripts varying by stage in accordance with their relative RNA content[10].

To identify differences resulting from *ap2-g* expression during the commitment cycle, we used an AP2-G knockdown parasite line in which the endogenous *ap2-g* coding sequence is fused to a destabilization domain that targets the resulting fusion protein for degradation in the absence of the stabilizing Shield1 ligand[4]; this line is hereafter referred to as AP2-G-DD.

During the commitment cycle, synchronized parasites were grown at high parasitaemia to favour sexual commitment[11] in the presence of either the ligand (treated) or solvent control (untreated). We sequenced a total of 12,800 infected erythrocytes that were isolated during the commitment cycle at 30, 36, and 42 h post-invasion (hpi), as well as nascent gametocytes (stage I) after 42 h of development in the subsequent cycle (see Methods and Extended Data Fig. 2). In two independent experiments, the average sexual commitment was found to be 17.5 ± 0.1% (mean ± s.e.m.) in treated cells while no gametocytes were observed in untreated cells (less than 0.05%).

After unsupervised clustering on the basis of similarity in overall gene expression[12], the 10,509 quality-filtered SCTs self-organized in a continuous arc consisting of 11 clusters (1–11) surrounding 5 central clusters (12–16) (Fig. 2a and Supplementary Video 1). Almost all cells in the cluster 1–11 continuum were isolated during the commitment cycle and self-organized primarily by time of collection (Fig. 2a and Extended Data Fig. 3). The centre clusters were composed of either stage I gametocytes (13–14) or cells from a mixture of time points (12, 15–16). Surprisingly, apart from the gametocyte clusters, no others showed notable enrichment for either treated or untreated cells (Extended Data Fig. 3c), suggesting that cell cycle progression was driving cluster assignment of SCTs irrespective of sexual commitment. This idea was further supported by a comparison of SCTs in clusters 1–11 to published, bulk RNA-seq time course data[13], which demonstrated that SCTs from progressively later clusters best matched an ordered series of time points (Fig. 2b and Extended Data Fig. 4a).

To test this hypothesis further, we applied the Monocle2 algorithm[14] to determine whether SCTs could be organized in a continuous gene expression program. Monocle-ordered SCTs also form a single continuum that recapitulates the cluster 1–11 order (Fig. 2c and Extended Data Fig. 4b). Finally, we ordered cells on the basis of progression through this continuum (noted in arbitrary pseudo-time units) and evaluated expression of gene sets associated with cell cycle progression and merozoite formation, beginning with DNA replication and ending with the expression of CDPK5, a calcium-dependent protein kinase that triggers merozoite egress[15] (Fig. 2d). Interestingly, post-mitotic schizonts occupied about two-thirds of this continuum, highlighting the tightly orchestrated transcriptional program necessary to assemble merozoite progeny over the final 8 h[16], following the earlier, relatively stable, activity of genome replication.

[1]Institute for Computational Biomedicine, Department of Physiology and Biophysics, Weill Cornell Medicine, New York, New York 10065, USA. [2]Caryl and Israel Englander Institute for Precision Medicine, Weill Cornell Medicine, New York, New York 10065, USA. [3]Physiology, Biophysics and Systems Biology Graduate Program, Weill Cornell Medicine, New York, New York 10065, USA. [4]Biochemistry, Cell & Molecular Biology Graduate Program, Weill Cornell Medicine, New York, New York 10065, USA. [5]Department of Microbiology & Immunology, Weill Cornell Medicine, New York, New York, USA. [6]Division of Hematology & Medical Oncology, Department of Medicine, Weill Cornell Medicine, New York, New York 10065, USA. [7]Immunology and Microbial Pathogenesis Graduate Program, Weill Cornell Medicine, New York, New York 10065, USA.
*These authors contributed equally to this work.

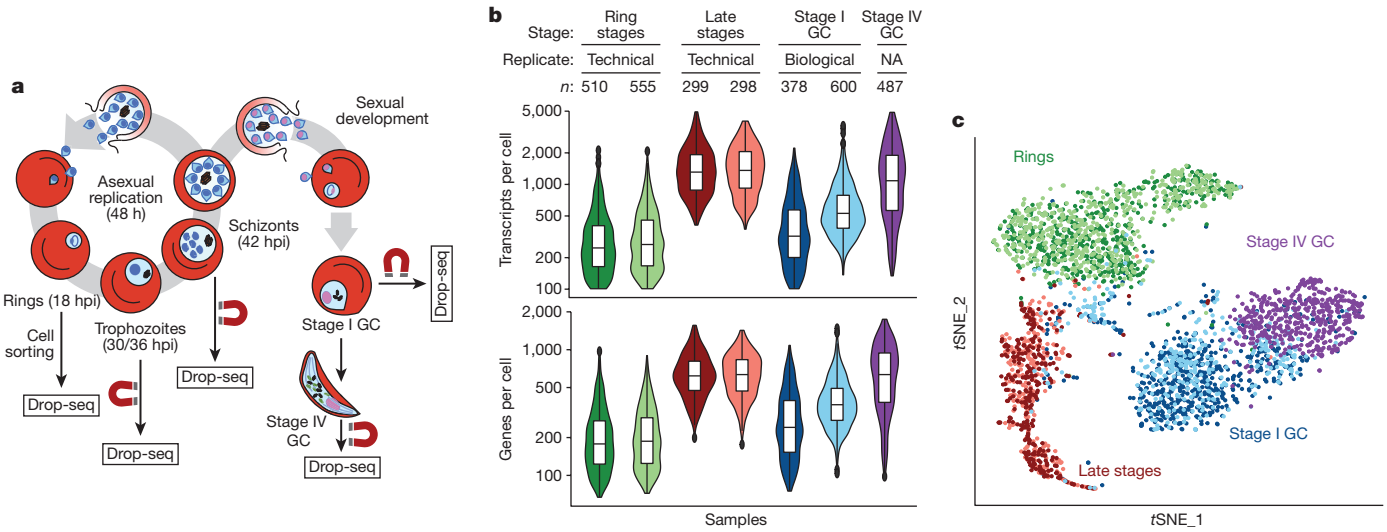

Figure 1 | Single-cell RNA-seq differentiates between *P. falciparum* life-cycle stages in a reproducible manner. a, Single-cell transcriptomes were collected from early (ring) and late asexual blood stages, as well as stage I and stage IV gametocytes (GC). Drop-seq, droplet-based single-cell mRNA sequencing. **b**, Distributions of unique transcripts per cell and detected genes per cell for collected stages across technical and biological replicates. NA denotes not applicable (that is, single experiment). The number of cells (n) in each sample is shown. Boxes indicate the interquartile range; whiskers extend 1.5× interquartile range from the box. **c**, t-distributed stochastic neighbour embedding (tSNE) map of 2,829 quality-filtered, single-cell transcriptomes collected from four parasite blood stages. Colours match experiments shown in **b**.

The processes of genome replication and merozoite formation are shared by both asexually and sexually committing parasites. Accordingly, cell cycle progression was the primary driver of cluster assignment, regardless of the underlying program of sexual commitment. This is consistent with the presence of *ap2-g* expressing sub-populations of treated cells within each of these 11 clusters (Fig. 3a). Over the 24–48 h window, mean *ap2-g* expression and the fraction of AP2-G-expressing (AP2-G$^+$) cells in both treated and untreated cells rises to a moderate peak in cluster 3 before falling again in cluster 4 (Fig. 3b). However, only when AP2-G activity was stabilized by ligand treatment did the abundance of *ap2-g* transcripts rise rapidly, reaching a maximal 22-fold increase (over cluster 1) in mature schizonts. The expression of *ap2-g* is significantly higher in treated than in untreated cells across clusters 1–11. Analysis of SCTs from 3,643 wild-type (NF54) schizonts (36–48 hpi) recapitulated these findings whether clustered independently or in conjunction with AP2-G-DD SCTs (Extended Data Fig. 5).

Rather than averaging gene expression across the entire population, which is heterogeneous with respect to cell cycle progression and commitment, our single-cell resolution allowed us to compare gene expression directly in cells expressing AP2-G (AP2-G$^+$) and in cells in which the locus remains silenced (AP2-G$^-$). This was made possible only by the large number of SCTs collected, which yielded many AP2-G$^+$ cells within each cluster and thereby provided sufficient statistical power to determine AP2-G-dependent differential gene expression.

Using this approach, we identified 19 genes that were significantly upregulated in AP2-G$^+$ late stage cells within at least one cluster of both treated AP2-G-DD (27 genes) and NF54 (48 genes) late stage cells (Fig. 3c, d, Extended Data Fig. 6 and Supplementary Table 3). In line with our previous observations that AP2-G acts as a transcriptional activator[4], almost all of the differentially expressed genes were upregulated in AP2-G$^+$ cells containing an average of 2.6 AP2-G-binding sites (3.8× fold enrichment, $P < 2 \times 10^{-6}$) within their upstream regions compared with 0.7 binding sites genome-wide. The number of upstream binding sites correlated well with the observed increase in AP2-G$^+$ cells (Spearman's $r = 0.52$). Six of these shared hits have been linked to interaction with the host cell either via protein export or during the reinvasion process, whereas seven putatively function in gene regulation on the basis of their predicted interaction with RNA, DNA or chromatin. These included two additional Apicomplexan AP2 (ApiAP2) family members, PF3D7_1139300 and PF3D7_1222400, a primate-specific ApiAP2 recently found to acquire loss-of-function mutations in laboratory-adapted strains[17]. Four additional hits are implicated in the regulation of chromatin structure: two SNF2 family helicases (ISWI and SNF2L) that function in chromatin remodelling[18], and two putative histone modifying enzymes (histone deacetylase HDA1[7], and the previously un-annotated putative histone lysine-specific demethylase *P. falciparum* LSD2, PF3D7_0801900)[19] (Extended Data Fig. 7).

Next, we explored the temporal dynamics of upregulation in AP2-G$^+$ cells for our 19 hits (Fig. 4a, b and Extended Data Fig. 8). Both of the putative SNF2 helicases are more highly expressed in AP2-G$^+$ cells when DNA replication remains ongoing (pseudo-time 0–20) preceding the initial rise in overall AP2-G expression. After its peak expression in trophozoites, the abundance of the AP2 transcript PF3D7_1222400 initially falls but rises again in AP2-G$^+$ cells (pseudo-time 20–35) immediately after the initial wave of AP2-G expression. AP2-G transcript abundance increases steadily during schizont segmentation (pseudo-time 30–50), leading to a sharp rise in the expression of LSD2, HDA1 and AP2 PF3D7_1139300 just before egress, as indicated by PFCDPK5 expression (pseudo-time > 50). The expression of shared hits in untreated AP2-G-DD cells mirrors the expression in treated AP2-G$^-$ cells. This demonstrates that the altered expression in AP2-G$^+$ cells depends on AP2-G activity. We confirmed AP2-G-dependent upregulation of the hits in late schizonts by quantitative PCR with reverse transcription (qRT–PCR) (Extended Data Fig. 9a) and RNA fluorescence *in situ* hybridization (FISH) (Fig. 4c, d and Extended Data Fig. 9b).

Because AP2-G is expected to bring about the coordinated expression of a limited set of genes, either directly or indirectly, we wanted to define a network of co-expressed genes in committed schizonts that is centred on AP2-G. To this end, we took advantage of our ability to determine true co-expression (within the same cell) to identify genes that are significantly co-expressed with AP2-G or any of our 19 hits across clusters 1–11 (Extended Data Fig. 10 and Supplementary Table 4). We relied on the recurrence of co-expressed gene pairs across all clusters to define a highly interconnected, AP2-G-centred network of significantly co-expressed genes (Fig. 4e).

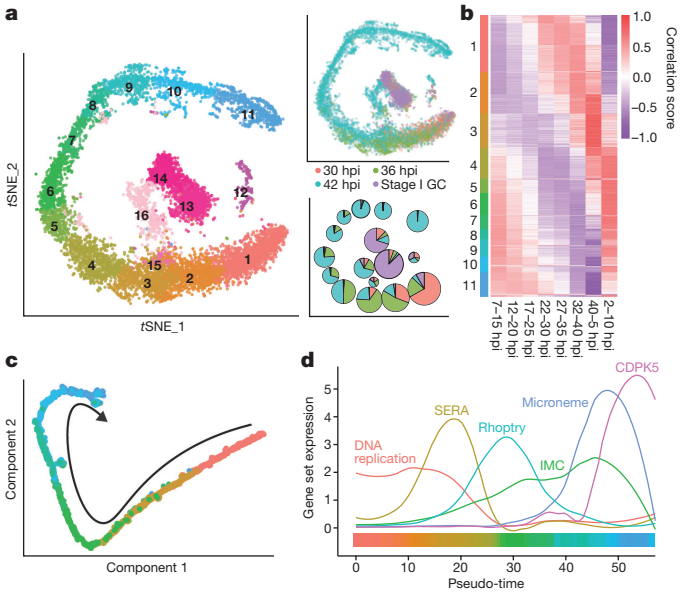

Figure 2 | Single cell RNA-seq of malaria parasites successfully captures cell cycle progression and differentiation. a, *t*SNE plots of SCTs collected from AP2-G-DD parasites at three asexual time points, and stage I gametocytes coloured by cluster assignment (left) or collection time (top right). Bottom right plot depicts cluster composition by collection time. **b**, Correlation of SCTs in clusters 1–11 (rows) to a bulk RNA-seq time course (columns). **c**, Dimensionality-reduction and pseudo-time ordering of the SCTs assigned to clusters 1–11 (colour). **d**, Scaled expression level of specific parasitic gene modules as a function of pseudo-time. Colour bar indicates average cluster assignment along pseudo-time. IMC, inner membrane complex proteins; SERA, serine-repeat antigen proteins.

Owing to its stochastic nature, transcriptional regulation of sexual commitment is uniquely suited for exploration by single-cell transcriptomics. By comparing thousands of single-cell transcriptomes from wild-type NF54 and AP2-G-DD parasites, we identified a shared transcriptional sexual commitment program that is executed as they progress through schizogeny (Fig. 4f). This program is initiated by derepression of the *ap2-g* locus during DNA replication (pseudo-time 0–15), concomitant with increased expression of the SNF2 helicases ISWI and SNF2L in AP2-G^{+} cells, and may implicate these chromatin-remodelling factors in the replacement or repositioning of nucleosomes that maintain *ap2-g* silencing. As DNA replication concludes, we observed an initial increase in AP2-G expression regardless of AP2-G stabilization, suggesting that this initial rise is not dependent on AP2-G function, consistent with epigenetic derepression. After reaching an initial peak (around pseudo-time 20), AP2-G expression drops temporarily (around pseudo-time 28) before increasing steadily for the remainder of the cell cycle. Unlike the initial increase, this second wave of expression requires the stabilization of AP2-G, confirming the existence of a previously proposed positive transcriptional feedback loop[4] that is likely to be activated by the direct binding of AP2-G to the cognate motifs present within its own promoter.

Bi-stable transcriptional switches frequently regulate cell differentiation and prevent the mixed expression of incompatible developmental programs[20–23]. As AP2-G reaches an initial peak, a second, genomically adjacent AP2 (PF3D7_1222400) is upregulated in AP2-G-expressing cells. The period of increased PF3D7_1222400 expression coincides with a temporary drop in AP2-G expression. Combined with recent evidence that culture adaptation selects for loss-of-function mutations in both AP2-G and PF3D7_1222400; the genomic location and expression of PF3D7_1222400 raise the possibility that it may act as a sexual commitment checkpoint before activation of the feedback loop. Finally, as AP2-G reaches its peak expression immediately before egress, a third AP2 factor (PF3D7_1139300) is sharply upregulated along with the histone-modifying enzymes LSD2 and HDA1. We propose that in sexually committed schizonts these regulators act together to prepare the gene expression necessary for gametocyte development in the subsequent cell cycle and may have a possible role in mating type determination.

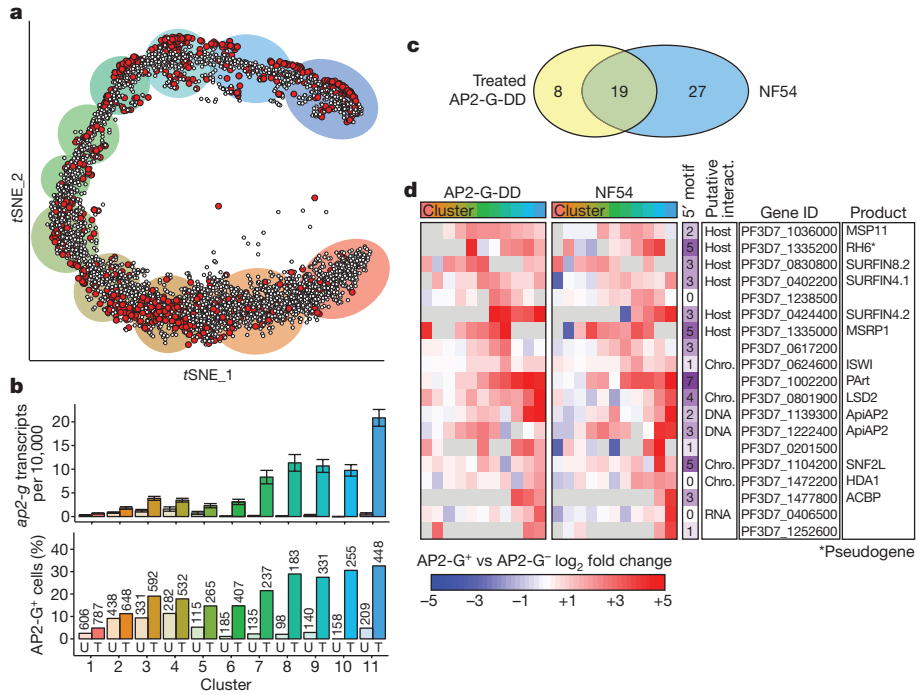

Figure 3 | AP2-G specific gene expression in committing parasites. a, In total, 19% of treated AP2-G-DD parasites expressed *ap2-g* (red). Colour outlines indicate cluster assignment. **b**, *ap2-g* expression in treated (T) and untreated (U) AP2-G-DD parasites by cluster. Mean expression (top) and percentage AP2-G^{+} (bottom) with number of cells indicated. Error bars are s.e.m. **c**, Number of differentially-expressed genes in treated AP2-G-DD and NF54 parasites. **d**, Differential gene expression in AP2-G^{+} versus AP2-G^{-} cells of shared hits in **c**, along with the number of upstream AP2-G-binding sites (purple) and putative interaction sites on the basis of annotation (host, host cell; chro., chromatin). Grey indicates that transcripts were not detected.

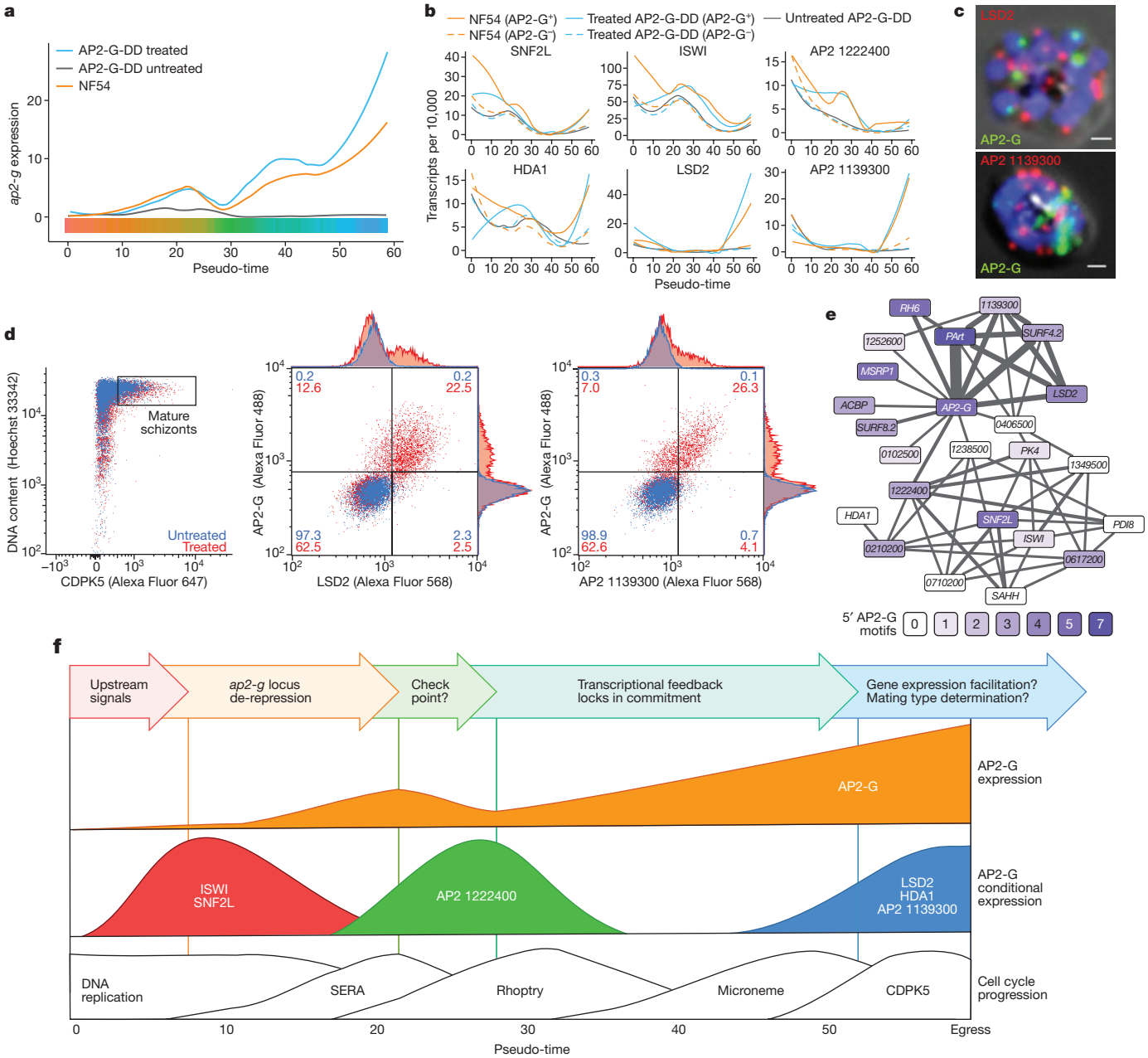

Figure 4 | Sexual commitment-specific expression. a, *ap2-g* expression in NF54 (orange), treated (blue), and untreated (grey) AP2-G-DD parasites versus pseudo-time. **b**, Gene expression in AP2-G^{+} (solid) and AP2-G^{-} (dashed) cells of NF54 (orange), treated AP2-G-DD (blue), and untreated AP2-G-DD (grey) cells. **c**, RNA FISH of AP2-G and LSD2 (top) or PF3D7_1139300 (bottom) in schizonts. DNA counterstained blue. Scale bars, 1 μm. **d**, Co-expression of AP2-G with LSD2 (middle) or PF3D7_1139300 (right) by RNA FISH in treated (red) and untreated (blue) mature schizonts based on DNA content and CDPK5 expression (shown in left panel, representative of three independent experiments). **e**, Co-expression network in sexually committed schizonts. Line thickness indicates number of clusters with co-expression. **f**, Model of transcriptional regulation during *P. falciparum* sexual commitment.

The ability to measure gene expression in thousands of individual parasites helps to address key questions that involve small sub-populations of parasites, such as the mechanisms underlying antigenic switching[24] and artemisinin-induced dormancy in resistant parasites[25], with important implications for the treatment of malaria and the development of vaccines.

Online Content Methods, along with any additional Extended Data display items and Source Data, are available in the online version of the paper; references unique to these sections appear only in the online paper.

Received 3 March; accepted 18 September 2017.
Published online 25 September 2017.

1. Cowman, A. F., Healer, J., Marapana, D. & Marsh, K. Malaria: biology and disease. *Cell* **167,** 610–624 (2016).
2. Silvestrini, F., Alano, P. & Williams, J. L. Commitment to the production of male and female gametocytes in the human malaria parasite *Plasmodium falciparum*. *Parasitology* **121,** 465–471 (2000).
3. Bruce, M. C., Alano, P., Duthie, S. & Carter, R. Commitment of the malaria parasite *Plasmodium falciparum* to sexual and asexual development. *Parasitology* **100,** 191–200 (1990).
4. Kafsack, B. F. C. *et al.* A transcriptional switch underlies commitment to sexual development in malaria parasites. *Nature* **507,** 248–252 (2014).
5. Sinha, A. *et al.* A cascade of DNA-binding proteins for sexual commitment and development in *Plasmodium*. *Nature* **507,** 253–257 (2014).
6. Brancucci, N. M. B. *et al.* Heterochromatin protein 1 secures survival and transmission of malaria parasites. *Cell Host Microbe* **16,** 165–176 (2014).

7. Coleman, B. I. *et al.* A *Plasmodium falciparum* histone deacetylase regulates antigenic variation and gametocyte conversion. *Cell Host Microbe* **16,** 177–186 (2014).
8. Pellé, K. G. *et al.* Shared elements of host-targeting pathways among apicomplexan parasites of differing lifestyles. *Cell. Microbiol.* **17,** 1618–1639 (2015).
9. Macosko, E. Z. *et al.* Highly parallel genome-wide expression profiling of individual cells using nanoliter droplets. *Cell* **161,** 1202–1214 (2015).
10. Sims, J. S. *et al.* Patterns of gene-specific and total transcriptional activity during the *Plasmodium falciparum* intraerythrocytic developmental cycle. *Eukaryot. Cell* **8,** 327–338 (2009).
11. Fivelman, Q. L. *et al.* Improved synchronous production of *Plasmodium falciparum* gametocytes *in vitro*. *Mol. Biochem. Parasitol.* **154,** 119–123 (2007).
12. Satija, R., Farrell, J. A., Gennert, D., Schier, A. F. & Regev, A. Spatial reconstruction of single-cell gene expression data. *Nat. Biotechnol.* **33,** 495–502 (2015).
13. Kensche, P. R. *et al.* The nucleosome landscape of *Plasmodium falciparum* reveals chromatin architecture and dynamics of regulatory sequences. *Nucleic Acids Res.* **44,** 2110–2124 (2016).
14. Qiu, X. *et al.* Single-cell mRNA quantification and differential analysis with Census. *Nat. Methods* **14,** 309–315 (2017).
15. Dvorin, J. D. *et al.* A plant-like kinase in *Plasmodium falciparum* regulates parasite egress from erythrocytes. *Science* **328,** 910–912 (2010).
16. Bozdech, Z. *et al.* The transcriptome of the intraerythrocytic developmental cycle of *Plasmodium falciparum*. *PLoS Biol.* **1,** e5 (2003).
17. Claessens, A., Affara, M., Assefa, S. A., Kwiatkowski, D. P. & Conway, D. J. Culture adaptation of malaria parasites selects for convergent loss-of-function mutants. *Sci. Rep.* **7,** 41303 (2017).
18. Narlikar, G. J., Sundaramoorthy, R. & Owen-Hughes, T. Mechanisms and functions of ATP-dependent chromatin-remodeling enzymes. *Cell* **154,** 490–503 (2013).
19. Volz, J. *et al.* Potential epigenetic regulatory proteins localise to distinct nuclear sub-compartments in *Plasmodium falciparum*. *Int. J. Parasitol.* **40,** 109–121 (2010).
20. Park, B. O., Ahrends, R. & Teruel, M. N. Consecutive positive feedback loops create a bistable switch that controls preadipocyte-to-adipocyte conversion. *Cell Rep.* **2,** 976–990 (2012).
21. Laurent, M. & Kellershohn, N. Multistability: a major means of differentiation and evolution in biological systems. *Trends Biochem. Sci.* **24,** 418–422 (1999).
22. Chickarmane, V., Troein, C., Nuber, U. A., Sauro, H. M. & Peterson, C. Transcriptional dynamics of the embryonic stem cell switch. *PLoS Comput. Biol.* **2,** e123 (2006).
23. Bhattacharya, S. *et al.* A bistable switch underlying B-cell differentiation and its disruption by the environmental contaminant 2,3,7,8-tetrachlorodibenzo-*p*-dioxin. *Toxicol. Sci.* **115,** 51–65 (2010).
24. Guizetti, J. & Scherf, A. Silence, activate, poise and switch! Mechanisms of antigenic variation in *Plasmodium falciparum*. *Cell. Microbiol.* **15,** 718–726 (2013).
25. Hott, A. *et al.* Artemisinin-resistant *Plasmodium falciparum* parasites exhibit altered patterns of development in infected erythrocytes. *Antimicrob. Agents Chemother.* **59,** 3156–3167 (2015).

Supplementary Information is available in the online version of the paper.

Acknowledgements We would like to thank the WCM Genomics and Flow Cytometry core facilities, and G. Suppa for technical assistance. This work was supported by WCM internal startup funds (B.F.C.K.) and the NSF CAREER award (DBI-10549646, to O.E.), LLS SCOR (7006-13 and 7012016, O.E.), Hirschl Trust Award (O.E.), Starr Cancer Consortium (I6-A618, to O.E.) and NIH 1R01CA194547 (O.E.). A.P. and C.N. were supported by WCM graduate fellowships.

Author Contributions B.F.C.K. conceived the study with input from O.E. B.F.C.K. performed culturing and sample preparation for a single initial Drop-seq experiment. A.P. established and optimized the Drop-seq platform in the laboratory of O.E., and carried out Drop-seq and library preparation. C.N. carried out all other parasite culturing and sample processing for Drop-seq and RNA FISH. O.A. assisted in library preparation. N.M.-T. aided in probe design, optimization of RNA FISH, and performed flow cytometry. M.L.G. aided in optimization of flow cytometry for RNA FISH, and D.C.H. suggested methods for RNA FISH and supervised N.M.-T. C.T.H. acquired RNA FISH micrographs. A.P. and B.F.C.K. developed and performed bioinformatic analyses with contributions from C.N. B.F.C.K. analysed flow cytometry data. B.F.C.K. and A.P. wrote the manuscript, designed and generated figures, with notable input by C.N. and O.E.

Author Information Reprints and permissions information is available at www.nature.com/reprints. The authors declare no competing financial interests. Readers are welcome to comment on the online version of the paper. Publisher's note: Springer Nature remains neutral with regard to jurisdictional claims in published maps and institutional affiliations. Correspondence and requests for materials should be addressed to B.F.C.K. (bjk2007@med.cornell.edu) or O.E. (ole2001@med.cornell.edu).

METHODS

Parasites and strains. The strains of parasite used in this study were AP2-G-DD[4], NF54, and DCJ[26]. They were maintained using established cell culture techniques[27]. Cultures were tested for mycoplasma every six months and found to be negative. Engineered strains were obtained from their laboratory of origin and tested for the engineered phenotype and expected drug-resistance. Specifically, DCJ parasites were resistant to blasticidin-S when tested in spring 2016. AP2-G-DD parasites were resistant to WR99210 and produced wild-type (NF54) levels of gametocytes when cultured in the presence of 0.5 μM Shield1 ligand but not when cultured with solvent control (tests performed in June 2017).

Gametocyte induction. For synchronous gametocyte induction[11], parasites were double-synchronized with 5% sorbitol solution[27] to achieve a synchrony of ±6 h and cultured while shaking (3% haematocrit). Synchronized parasites were set up at 2% late trophozoite stage. After re-invasion, parasites were maintained at 7–8% parasitaemia during the commitment cycle to induce sexual commitment. Once parasites reached the schizont stage, they were expanded 1:4 in order to relieve stress. After re-invasion, on the first day of gametocyte development (D + 1), ring-stage parasites were counted and treated with 50 mM *N*-acetyl-D-glucosamine[27] for three consecutive days to kill asexuals, and gametocytaemia was counted on the fourth day of gametocyte development (D + 4). The gametocyte commitment rate was then determined by dividing the D + 4 gametocytaemia by the D + 1 parasitaemia, counted before addition of *N*-acetyl-D-glucosamine.

Parasite isolation for single-cell (sc) RNA-seq. AP2-G-DD or NF54 parasites were set up for gametocyte induction as described above. For AP2-G-DD, the cultures were split in two after re-invasion on D − 2 was completed and treated with 0.5 μM Shield1 or an equal volume of ethanol solvent for the remainder of the experiment[28]. Infected erythrocytes were purified at the desired developmental time-point (on D − 1: 30, 36 and 42 hpi; on D + 2: 42 h into gametocyte development) using magnetic columns (LS columns, Miltenyi Biotec)[27]. On the magnet, columns were washed with media without AlbuMAX, after which the parasite culture was loaded. After washing with media without AlbuMAX and with 0.01% BSA in PBS, haemozoin-containing parasites were eluted off the magnet with 0.01% BSA in PBS. The sample was adjusted to 1.3×10^5 cells per ml, kept on ice and immediately subjected to Drop-seq.

DCJ parasites were cultured in media supplemented with 5 μg ml^{-1} blasticidin-S. Synchronized parasites at 18 ± 4 hpi were then stained at 1% haematocrit with 2 μM Hoechst 33342 for 10 min at room temperature, pelleted and re-suspended in colourless media without AlbuMAX to 0.1% haematocrit. Hoechst 33342-positive cells were sorted into 0.01% BSA in PBS using a FACSAria II sorter (BD Biosciences), adjusted to a concentration of 1.3×10^5 cells per ml, kept on ice and immediately subjected to Drop-seq. All samples were inspected by microscopy and only used for scRNA-seq if singly infected red blood cells (RBCs) made up >95% of the total.

Please see Supplementary Table 1 for the number for samples collected.

Parasite isolation for RNA FISH and qRT–PCR. Schizonts of semi-synchronous AP2-G-DD parasites were isolated using a Percoll–sorbitol gradient and reintroduced into culture with fresh blood at 4% parasitaemia. After 6 h shaking in culture, the remaining schizonts were removed using 5% sorbitol lysis, leaving a tightly synchronous population of early ring stages at high parasitaemia as desired for induction of sexual commitment (0–6 hpi, 4–7% parasitaemia). The culture was immediately split in two and supplemented with either 0.5 μM Shield1 ligand or solvent control for the remainder of the experiment[28]. After 45 h, when the parasites were midway through re-invasion, highly synchronous mature schizonts were magnetically isolated as described above and used for RNA FISH or bulk RNA extraction for qRT–PCR.

RNA FISH and detection. RNA FISH was carried out using PrimeFlow (ThermoFisher) according to the manufacturer's instructions and stained for DNA with Hoechst 33342. Custom probes were designed and synthesized against unique regions of the AP2-G (Alexa Fluor 488), CDPK5 (Alexa Fluor 647), LSD2 (Alexa Fluor 568) and AP2 PF3D7_1139300 (Alexa Fluor 568) transcripts by the manufacturer (Supplementary Table 5). Detection was carried out using a BD LSR II flow cytometer using 350 nm, 488 nm, 561 nm and 650 nm lasers, respectively. To ensure analysis of individual parasites, a single uniform population of parasites (RBC membranes are removed during fixation/permeabilization) was triple gated on forward scatter (FSC)-A versus side scatter (SSC)-A, FSC-H versus FSC-A and SSC-H versus SSC-A. Fluorescence gates were set using fluorescence-minus-one controls (see Extended Data Fig. 9). Mature schizonts, as identified by maximal DNA content and high CDPK5 expression, were analysed for expression of AP2-G and either LSD2 or PF3D7_1139300.

Microscopy. Cells were imaged as *z*-stacks on a Leica DMI6000 microscope at 1000× magnification using differential interference contrast optics and DAPI, GFP and Cy3 filter cubes to detect Hoechst-33342, Alexa Fluor 488 and Alexa Fluor 536, respectively. Fluorescent channel *z*-stacks were deconvolved using the ImageJ DeconvolutionLab2 plugin (NLLS algorithm) followed by maximum intensity *z*-projection and background adjustment.

qRT–PCR. Trizol-extracted RNA from saponin-lysed parasites (0.1% in PBS) was used for cDNA synthesis with random hexamers using SuperScript II (ThermoFisher) according to the manufacturer's instructions. Quantitative PCR was performed using gene-specific primer sets (Supplementary Table 6) and iTaq Universal SYBR Green Supermix (Bio-Rad). Relative transcript abundance was determined by normalizing to expression levels of fructose-biphosphate aldolase (PF3D7_1444800) using the $\Delta\Delta C_t$ method[29].

Drop-seq and sequencing analysis pipeline. Single-cell transcriptomic profiles were generated using Drop-seq, a technology designed for highly parallel genome-wide expression profiling of individual cells using nanolitre droplets, as previously described[9]. In brief, single-cell suspensions and uniquely barcoded beads were colocalized in droplets using a microfluidics device (see CAD file from http://mccarrolllab.com/dropseq/, manufactured by FlowJEM). The droplets are composed of cell-lysis buffer and serve as compartmentalizing chambers for RNA capture. Flow rates were adjusted to maintain stable droplet formation and increase droplet homogeneity. We then adjusted cell and bead concentrations to accommodate variation in droplet size compared to the original publication[9] (113 μm in our system). Doublet rate was estimated with the species-mixing experiment described previously[9]. Examination of cells showed complete lysis within the time required for examination by microscopy (less than 1 min), notably shorter than the time cells spend in droplets during lysis and mRNA capture.

Droplet breakage and single-cell library preparations followed the procedure as described[9]. In brief, collected droplets were disrupted and RNA-hybridized beads were extracted. Reverse transcription was performed with template switching to allow for cDNA amplification by PCR. An additional pre-PCR step was added to determine the appropriate number of cycles (17–19 cycles) to achieve a cDNA library at a concentration of 400–1,000 μg μl^{-1}, as suggested by the protocol. cDNA samples were purified using Agencourt AMpure XP (Beckman Coulter), and were run on a 2100 BioAnalazyer instrument with a High Sensitivity DNA kit (Agilent Technologies). Samples were prepared for sequencing using the Illumina Nextera XT kit, and sequenced on a NextSeq 500 (Illumina) at an average of 70,000 reads per cell. Libraries with large numbers of cells were divided into technical replicates, which were processed independently. Raw reads were processed and aligned (STAR aligner) using the standard Drop-seq pipeline, and according to the 'Drop-seq Alignment Cookbook', both found at http://mccarrolllab.com/dropseq/. Reads were aligned to the *P. falciparum* 3D7 transcriptome (PlasmoDB v. 32). For each read, a single optimal mapping position was retained. Unique transcripts mapping to alternative splice variants were combined for subsequent analysis. Single-cell expression matrices were generated using cellular barcodes and unique molecular identifiers (UMIs). As Drop-seq RNA capture is designed for poly-adenylated transcripts, we removed known RNA pol I/III transcripts (rRNA, tRNA) before analysis. UMIs mapping to ribosomal RNA transcripts comprised less than 5% of reads for 99.5% of our cells. Even though individual malaria parasites contain significantly less RNA than mammalian cells[30], the average number of transcripts captured per asexual late-stage parasite or gametocyte was similar to that reported for mammalian cells[9], indicating higher capture efficiency. Transcript capture from ring-stage cells yielded 70–80% fewer UMIs compared to late-stage cells, reflecting the substantially lower RNA content of ring-stage cells compared to cells from late stages[30].

Single-cell transcriptome analysis. Data normalization, clustering and differential expression were performed using the Seurat R package[12]. Cells with less than 100 (ring-stages) or 300 (other stages) UMIs and genes detected in less than three cells were excluded from analysis. SCTs were internally normalized to 10,000 transcripts, log transformed and regressed on the number of UMIs per cell before dimensionality reduction and clustering. We selected ~600–700 highly variable genes using the expression and dispersion (variance/mean) of genes, and performed principle component analysis. The most significant principal components (20–30) were used for clustering and *t*SNE representations[31]. Clustering resolution was chosen such that visually distinct groups of more than 100 cells were assigned to individual clusters.

After filtering low expression genes, pseudo-temporal assignment was performed by applying the Monocle 2 R package to ~1,100 most variable genes to order the cells along pseudo-time.

SCT correlation with bulk RNA-seq. Mapping the cells from clusters 1–11 to the time series bulk RNA-seq dataset was performed by calculating the Pearson's correlation coefficient of each SCT with each of the 8 bulk-RNA-seq time points. The cells were ordered by their cluster number, and by the time point of maximal correlation.

Gene-module expression analysis. We defined modules of genes related to specific transcriptional programs activated during different stages of the cell cycle (Supplementary Table 2). We then summed the fraction of the transcriptome of

each cell for all the genes in each module. After normalization by the mean expression of each module across all cells, we plotted the LOESS-smoothed gene-module expression over pseudo-time.

Differential gene expression in AP2-G$^+$ versus AP2-G$^-$ cells. We used the Seurat package to calculate differential gene expression between treated AP2-G$^+$ cells and treated AP2-G$^-$ cells in each of clusters 1–11, and repeated this analysis for clusters 1–9 of the NF54 cells. We set several requirements: (1) that for each cluster treatment, groups contained more than 11 cells; (2) that the number of cells expressing a gene differed by at least 17.5% between treatment groups; (3) that genes are expressed in >10% of the cells of at least one treatment group; and (4) that gene expression differed >2.45-fold between treatment groups. Infinite ratios were capped at the maximal finite value observed. Figure 3d shows the fold change of the 19 genes found to be differentially expressed in both strains, across all 11 clusters of co-clustered AP2-G-DD and NF54 SCTs.

Co-expression analysis and network construction. For each of clusters 1–11 of the AP2-G-DD SCTs, we used the Fisher's exact test to detect significant co-expression between *ap2-g* and the 19 shared differentially expressed genes (Fig. 3b, d), and all other genes. We then used the Spearman's correlation coefficient and the mean square contingency coefficient of the same gene-pairs for filtering, requiring false discovery rate (FDR)-corrected *P* values from the Fisher's test to be less than 0.05 and agreement between the signs of the correlation coefficient and the mean square contingency coefficient. In addition, we required a mean square contingency coefficient greater than 0.3. The result is a table of significantly co-expressed genes in each cluster (Supplementary Table 4). For co-expression pairs repeating in 5 or more clusters, an undirected weighted network was constructed, in which edge weight is the number of occurrences of each gene pair. Networks were generated using the igraph R package[32] and visualized using Cytoscape[33].

AP2-G motif calling and enrichment testing. Upstream regions were defined as extending up to 3 kb from the ATG start codon. For intergenic regions of less than 6 kb containing promoters of two genes, exactly half of the intergenic sequence was assigned to each gene. Within these regions, putative AP2-G-binding sites were identified using SCANACE[34] and the 6-bp core position-specific weight matrix for AP2-G[35]. AP2-G motif enrichment analyses were performed using Fisher's exact test on the contingency table of motifs in the compared genes sets.

LSD2 Sequence analysis. The amino acid sequence of *Plasmodium falciparum* LSD2 was aligned with 4 other phylogenetically well-distributed syntenic *Plasmodium* orthologues (*P. vivax*, *P. ovale curtisi*, *P. gallinaceum*, *and P. berghei*) using the phylogeny-aware multiple sequence aligner webPRANK (https://www.ebi.ac.uk/goldman-srv/webprank/, Supplementary Data 1). Homologous blocks were joined and analysed for functional conservation using the NCBI Conserved Domain Database (https://www.ncbi.nlm.nih.gov/cdd/) and PANTHER (Protein ANalysis THrough Evolutionary Relationships, http://www.pantherdb.org/tools/) (Extended Data Fig. 7).

Other statistical analyses. Significance of mean differential gene expression across conditions (Fig. 3b) was assessed using two-sided Welch's two sample *t*-test, *P* values in multiple hypothesis testing are FDR corrected. Fisher's test was used to test significance of enrichment in AP2-G-binding sites. No statistical methods were used to predetermine sample size. The experiments were not randomized. The investigators were not blinded to allocation during experiments and outcome assessment.

Data availability. The scRNA-seq data of this study have been deposited in the NCBI Sequence Read Archive under accession code SRP116718. All other data are available from the corresponding authors upon reasonable request.

Code availability. The scripts used for analysis and figure generation are available at https://github.com/KafsackLab/scRNAseq-Malaria.

26. Dzikowski, R., Frank, M. & Deitsch, K. Mutually exclusive expression of virulence genes by malaria parasites is regulated independently of antigen production. *PLoS Pathog.* **2,** e22 (2006).
27. Moll, K., Ljungström, I., Perlmann, H. & Scherf, A. (eds) *Methods in Malaria Research* 5th edn (MR4/ATCC, 2008).
28. Armstrong, C. M. & Goldberg, D. E. An FKBP destabilization domain modulates protein levels in *Plasmodium falciparum*. *Nat. Methods* **4,** 1007–1009 (2007).
29. Livak, K. J & Schmittgen, T. D. Analysis of relative gene expression data using real-time quantitative PCR and the $2^{-\Delta\Delta C_t}$ method. *Methods* **25,** 402–408 (2001).
30. Martin, R. E., Henry, R. I., Abbey, J. L., Clements, J. D. & Kirk, K. The 'permeome' of the malaria parasite: an overview of the membrane transport proteins of *Plasmodium falciparum*. *Genome Biol.* **6,** R26 (2005).
31. Maaten, L. V. D. & Hinton, G. Visualizing data using *t*-SNE. *J. Mach. Learn. Res.* **9,** 2579–2605 (2008).
32. Csardi, G. & Nepusz, T. The igraph software package for complex network research. *InterJournal* http://www.interjournal.org/manuscript_abstract.php?361100992 (2006).
33. Lopes, C. T. *et al.* Cytoscape Web: an interactive web-based network browser. *Bioinformatics* **26,** 2347–2348 (2010).
34. Roth, F. P., Hughes, J. D., Estep, P. W. & Church, G. M. Finding DNA regulatory motifs within unaligned noncoding sequences clustered by whole-genome mRNA quantitation. *Nat. Biotechnol.* **16,** 939–945 (1998).
35. Campbell, T. L., De Silva, E. K., Olszewski, K. L., Elemento, O. & Llinás, M. Identification and genome-wide prediction of DNA binding specificities for the ApiAP2 family of regulators from the malaria parasite. *PLoS Pathog.* **6,** e1001165 (2010).

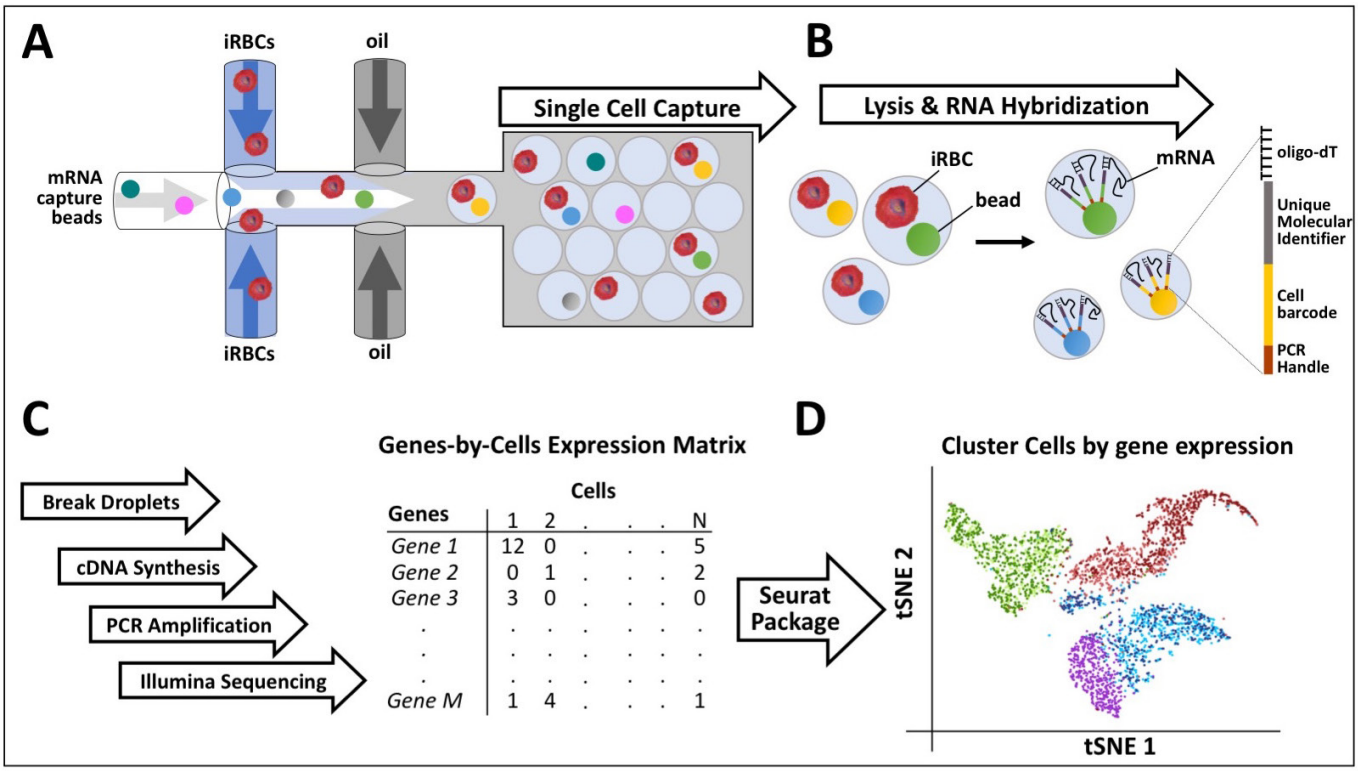

Extended Data Figure 1 | Drop-seq single-cell sequencing and analysis workflow. a, Single, infected RBCs (iRBCs) and uniquely barcoded beads are captured in droplets of cell lysis buffer using a microfluidics device. **b**, Released mRNAs are captured on individually barcoded poly-dT oligonucleotides. **c**, Template-switch cDNA synthesis labels each captured transcript with a cell-specific barcode and a unique molecular identifier (UMI). Following library preparation and Illumina sequencing, individual transcripts are mapped and counted within each cell. **d**, The resulting expression matrix of single-cell transcriptomes is used for clustering and analysis using the Seurat package of scRNA-seq analysis tools.

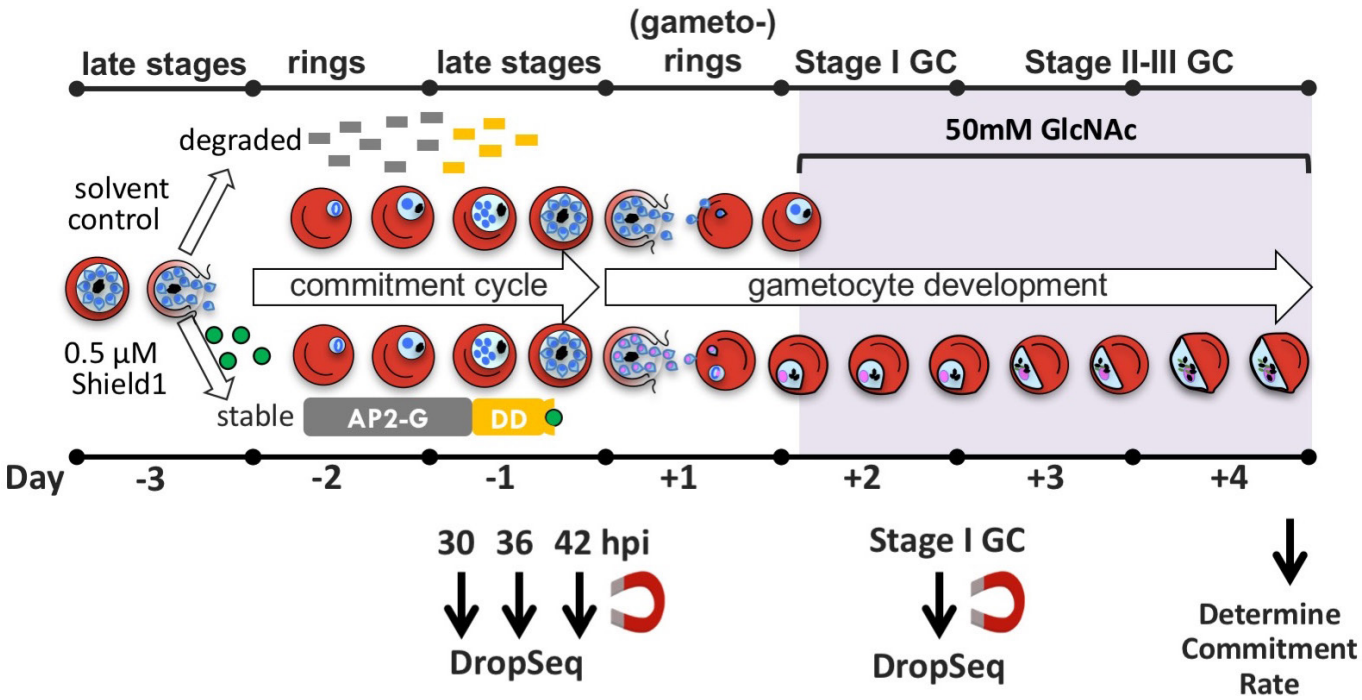

Extended Data Figure 2 | Experimental overview. Fusion of the endogenous *ap2-g* coding sequence with the FKBP destabilization domain (DD) makes sexual commitment conditional on treatment with 0.5 µM Shield1 ligand. Unless ligand is added, AP2-G is targeted for proteolytic degradation. At the start of the commitment cycle, AP2-G-DD parasites were split into two cultures and treated with ligand or solvent control. Cultures were maintained under conditions inducing sexual commitment and infected RBCs were purified for Drop-seq at 30, 36 and 42 hpi during the commitment cycle, and after 42 h of gametocyte development in the subsequent cycle.

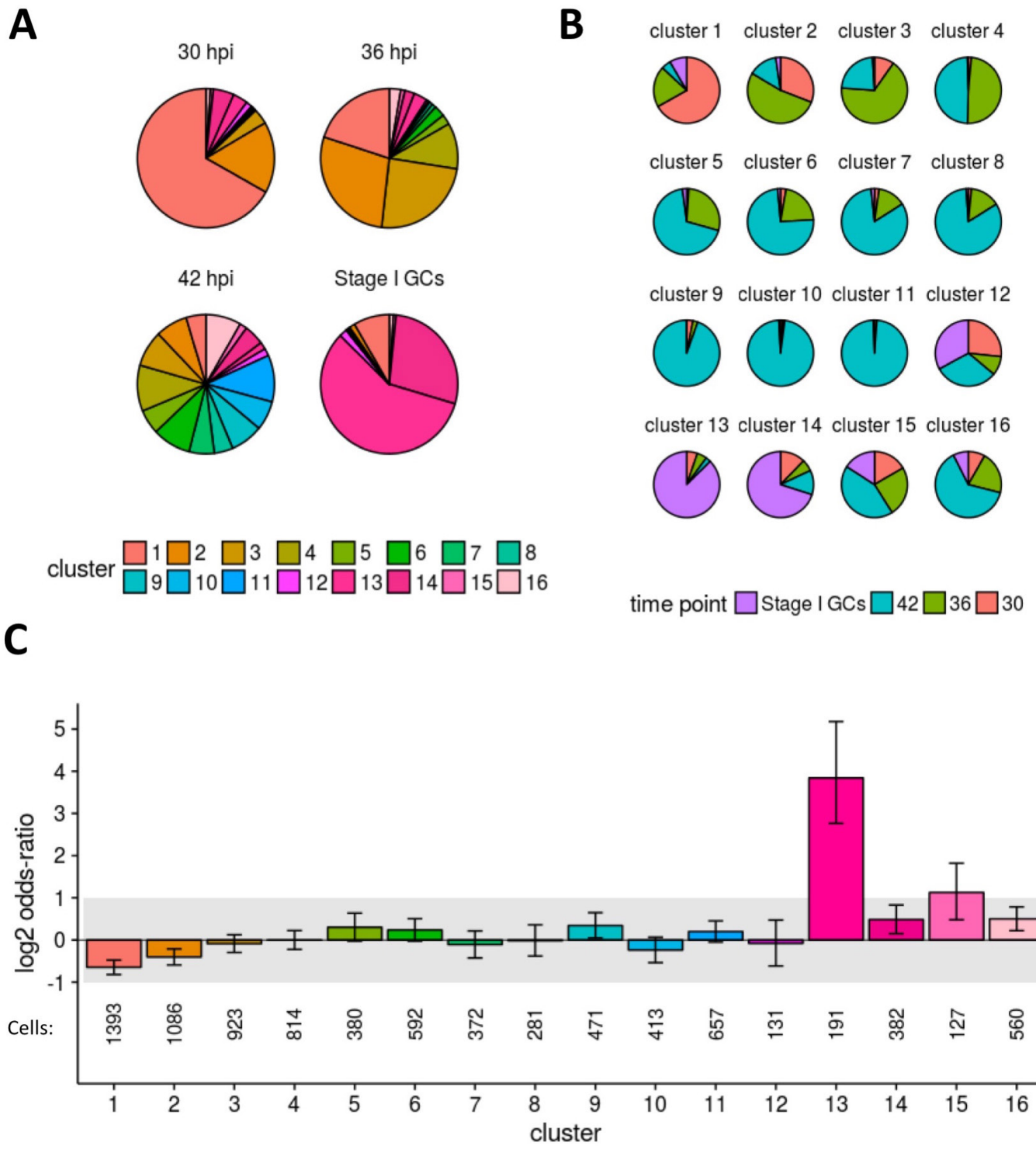

Extended Data Figure 3 | Analysis of AP2-G-DD cluster composition. **a**, Cluster assignment of SCTs collected at 30, 36, and 42 hpi and from stage I gametocytes. **b**, Cluster composition by sample time point. **c**, Cluster-wise enrichment for treated versus untreated cells collected during the commitment cycle. Positive and negative log-odds-ratio values indicate enrichment for treated and untreated cells, respectively. Error bars indicate the 95% confidence interval. The number of cells (*n*) in each sample is shown.

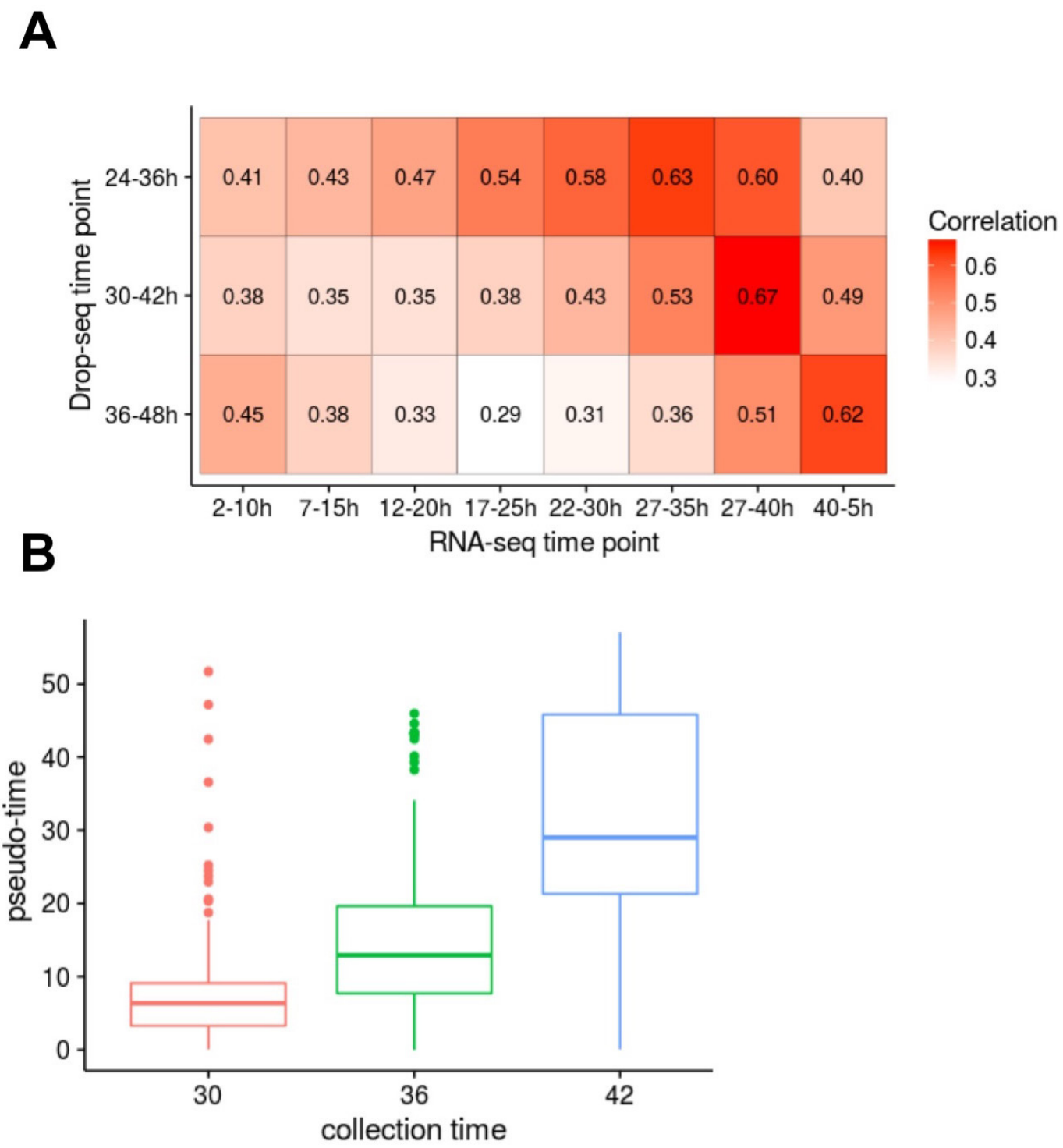

Extended Data Figure 4 | Single-cell transcriptomes averaged by collection time match corresponding bulk RNA-seq time points and pseudo-time assignment. a, The averaged single-cell expression profiles for each of the collected samples ($n_{24–36\,h} = 1{,}202$, $n_{30–42\,h} = 1{,}536$, $n_{36–48\,h} = 6{,}035$) were correlated with published bulk RNA-seq time points. Pearson's correlation coefficients are shown in heatmap boxes. Maximal correlation values indicate agreement between collection time point and transcriptome mapping. **b**, The distributions of pseudo-time assignment of treated cluster 1–11 SCTs grouped by collection time ($n_{30\,h} = 508$, $n_{36\,h} = 821$, $n_{42\,h} = 3{,}356$). Boxes indicate the interquartile range; whiskers extend 1.5× interquartile range from the box.

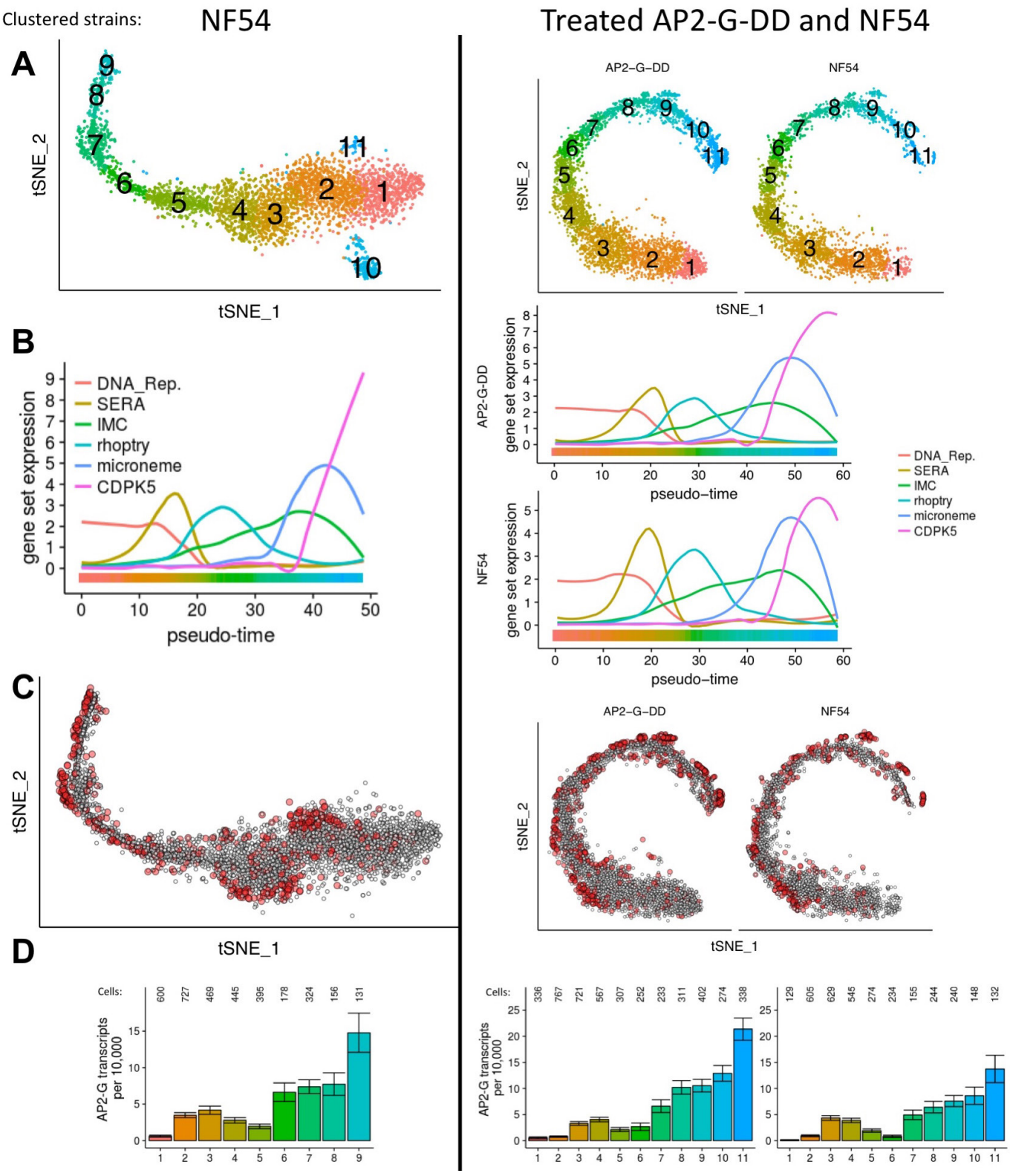

Extended Data Figure 5 | Analysis of NF54 late-stage SCTs clustered independently or co-clustered with treated AP2-G-DD SCTs. a–d, SCTs clustered independently (left) or co-clustered with treated AP2-GG-DD (right). **a**, *t*SNE plot of cluster 1–11 SCTs. **b**, Gene set expression as a function of pseudo-time. Colour bar indicates cluster assignment along pseudo-time. **c**, *t*SNE plot showing AP2-G^{+} cells in red. **d**, Mean *ap2-g* expression per 10,000 transcripts by cluster. Error bars are s.e.m. The number of cells (*n*) in each sample is shown.

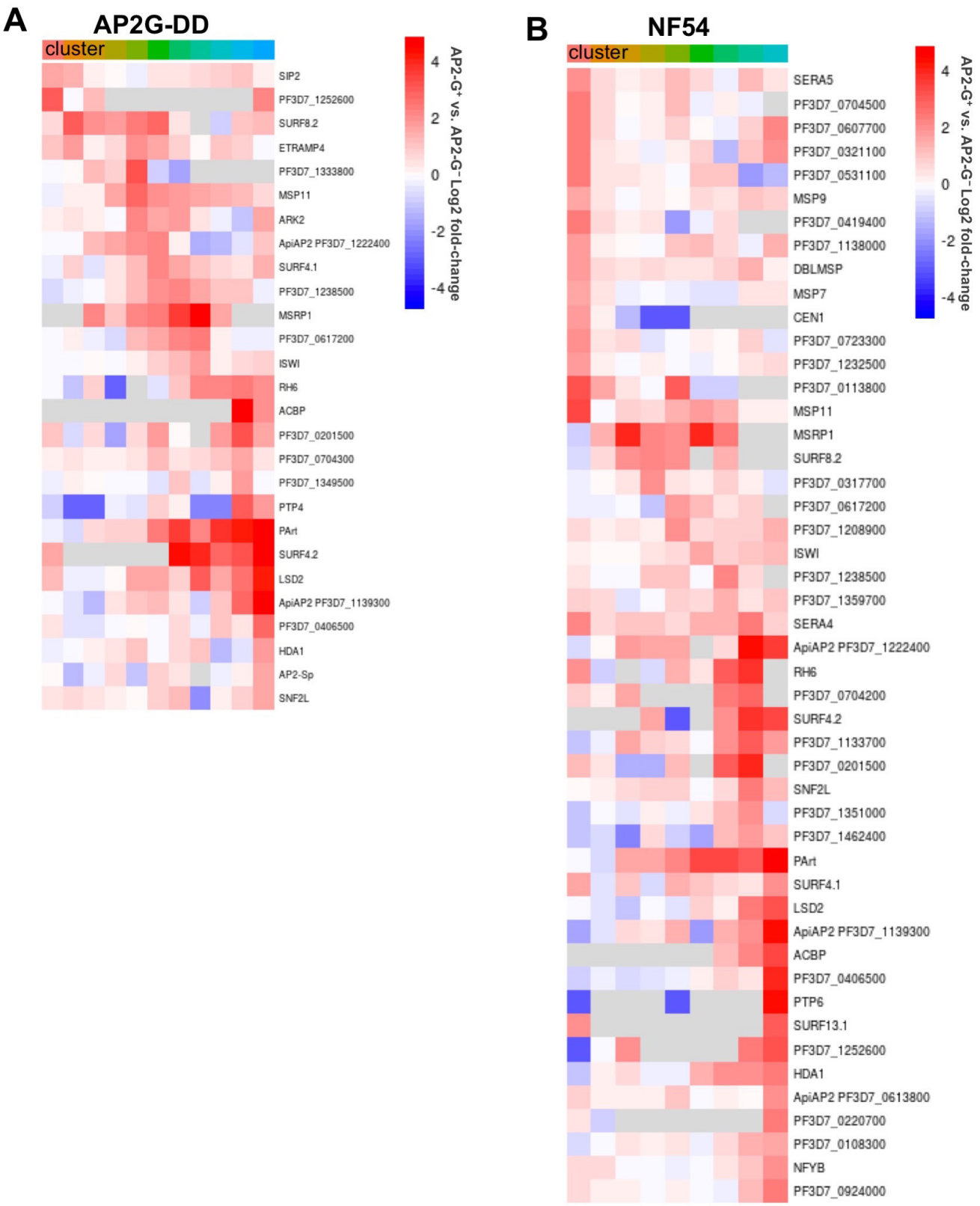

Extended Data Figure 6 | Differential expression analysis in treated AP2-G-DD and NF54 cells. a, **b**, The fold change of differentially expressed genes in treated AP2-G^{+} cells compared to AP2-G^{-} cells in AP2-G-DD SCTs (**a**) or independently clustered NF54 SCTs (**b**). Grey denotes not detected.

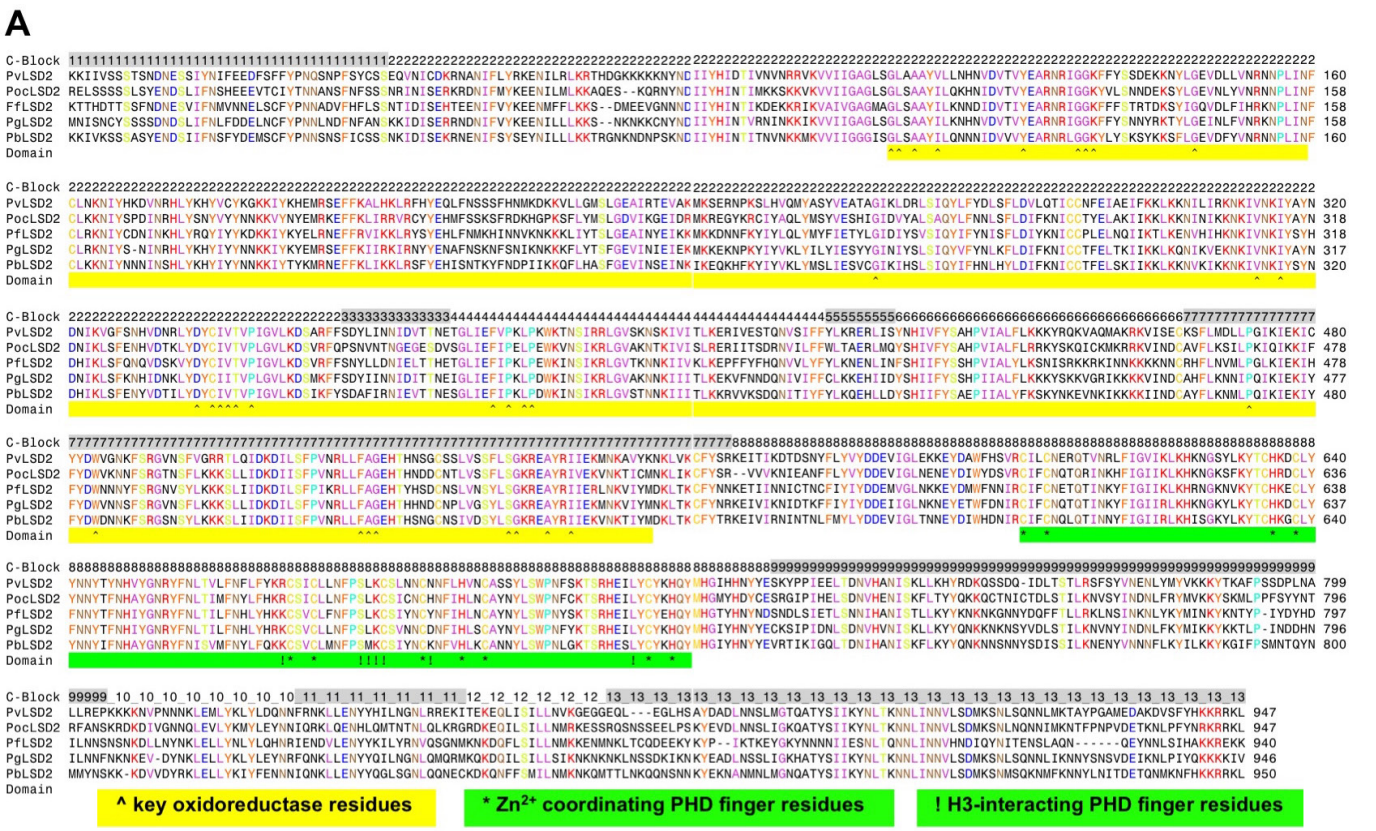

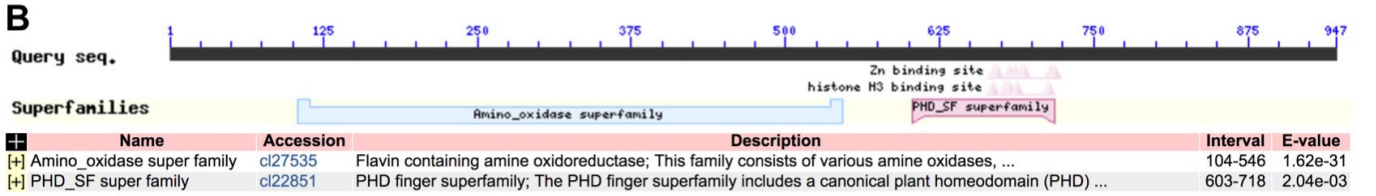

Name	Accession	Description	Interval	E-value
[+] Amino_oxidase super family	cl27535	Flavin containing amine oxidoreductase; This family consists of various amine oxidases, ...	104-546	1.62e-31
[+] PHD_SF super family	cl22851	PHD finger superfamily; The PHD finger superfamily includes a canonical plant homeodomain (PHD) ...	603-718	2.04e-03

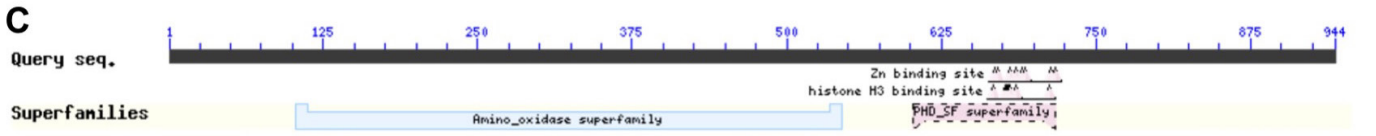

Name	Accession	Description	Interval	E-value
[+] Amino_oxidase super family	cl27535	Flavin containing amine oxidoreductase; This family consists of various amine oxidases, ...	103-545	2.07e-22
[+] PHD_SF super family	cl22851	PHD finger superfamily; The PHD finger superfamily includes a canonical plant homeodomain (PHD) ...	602-717	0.22

Extended Data Figure 7 | Homology-based functional annotation of PF3D7_0801900 as a putative histone lysine-specific demethylase. **a**, Alignment of conserved blocks (C-blocks) for *P. falciparum* (Pf) LSD2 (PF3D7_0801900) and syntenic orthologues in *P. vivax* (Pv) (PVP01_0118300), *P. ovale curtisi* (Poc) (PocGH01_01025900), *P. gallinaceum* (Pg) (PGAL8A_00078100), and *P. berghei* (Pb) (PBANKA_1228300). Coloured residues are conserved. Key functional residues for the flavin-containing amine oxidoreductase (PF01593, yellow) and extended plant homeodomain (PHD) finger (cd15571, green) domains are indicated. **b**, NCBI Conserved Domain Database hits for *P. vivax* LSD2 conserved blocks. **c**, NCBI Conserved Domain Database hits for *P. falciparum* LSD2 conserved blocks. **d**, Single PANTHER database functional annotation hit for *P. falciparum* LSD2 conserved blocks.

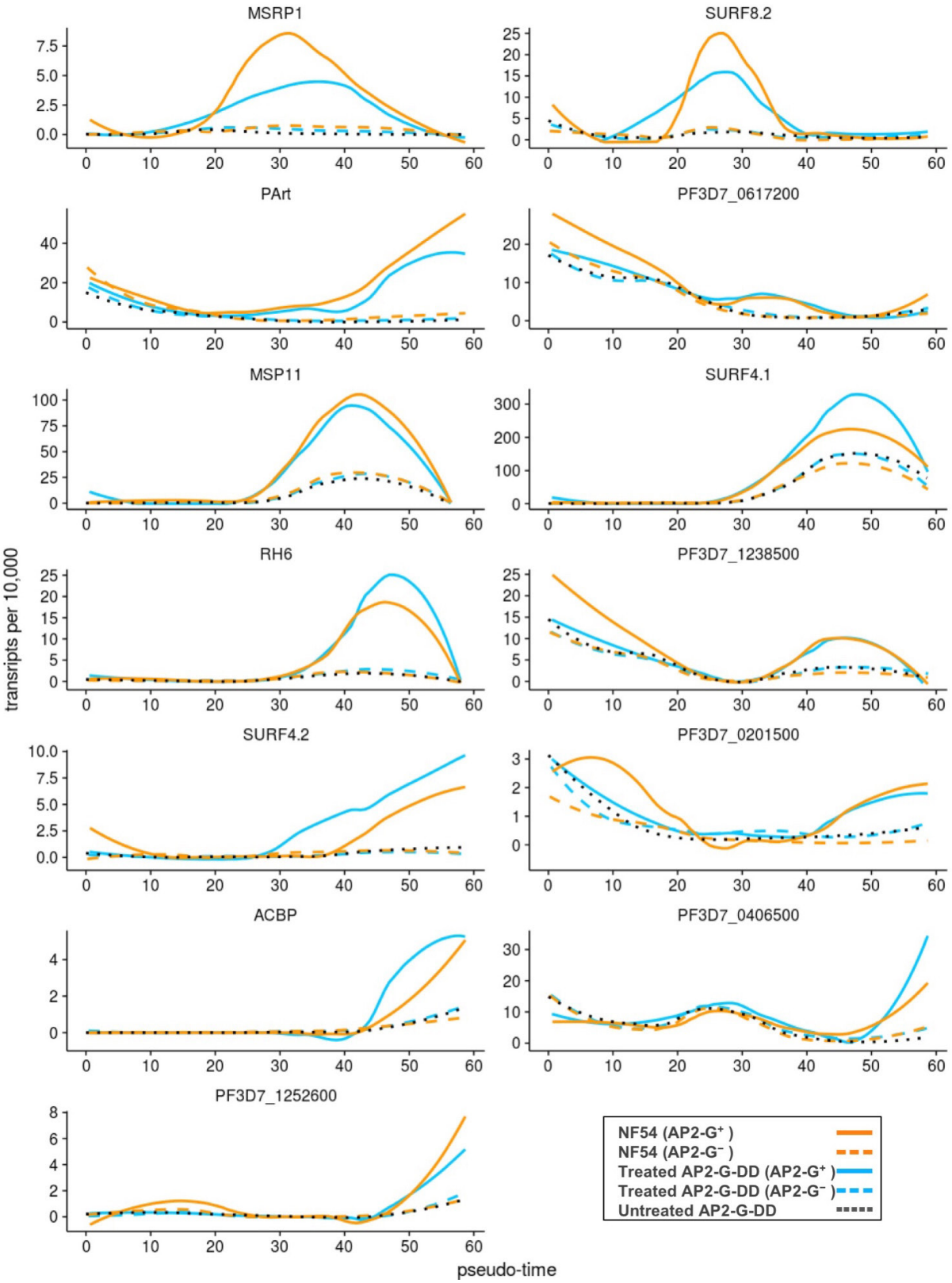

Extended Data Figure 8 | Differential expression of putative regulators. Expression in AP2-G$^+$ cells (solid) and AP2-G$^-$ cells (dashed) of NF54 (orange) and treated AP2-G-DD (blue) cells, as well as in untreated AP2-G-DD cells (dotted black) of Fig. 3d hits not shown in Fig. 4b.

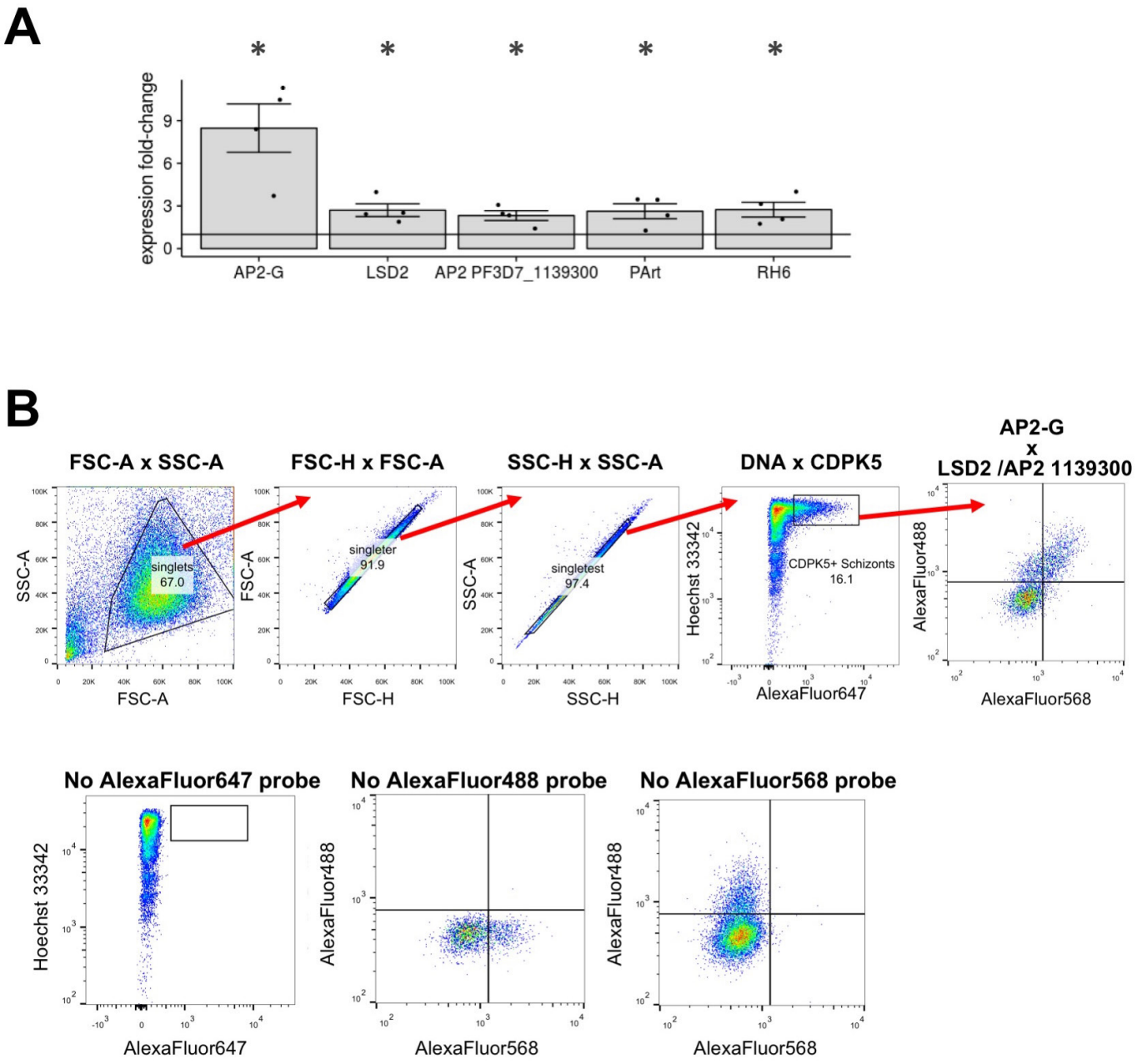

Extended Data Figure 9 | Validation of single cell findings. **a**, Fold change in expression of treated versus untreated AP2-G-DD schizonts as determined by qRT–PCR. Four independent biological replicates; the asterisk indicates significantly higher than 1.0 (one-sided $P < 0.05$, two-sided Welch's two-sample *t*-test). Bar height indicates the mean fold change across replicates, error bars are s.e.m. **b**, RNA FISH quantification gating schema (top) and fluorescence minus-one controls (bottom) for data shown in Fig. 4d. Results are representative of three independent experiments.

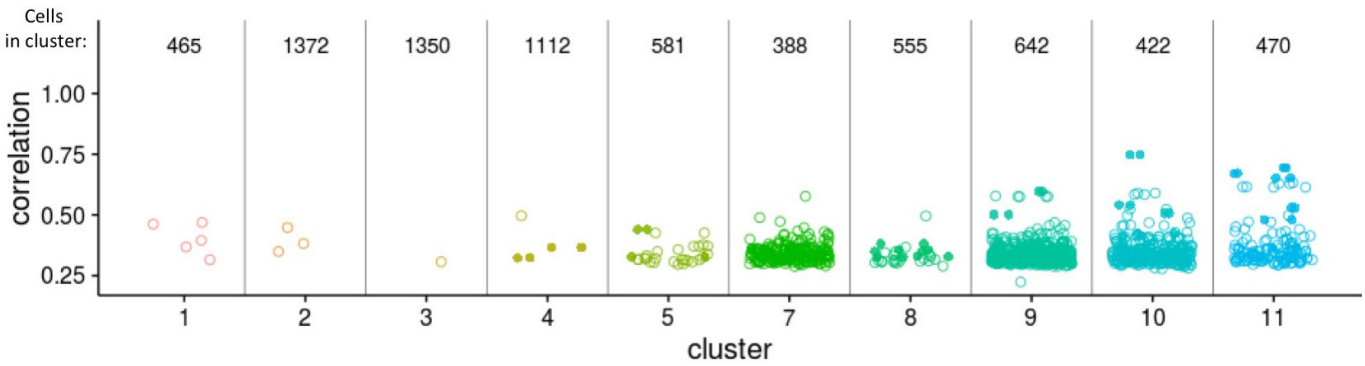

Extended Data Figure 10 | Expression correlation coefficients for pairs of significantly co-expressed genes by cluster. For each cluster, all genes across all the treated AP2-G-DD and NF54 cells in the cluster were evaluated for co-expression ($\phi > 0.3$) with each of the 19 shared hits in Fig. 3d. Spearman's correlation of expression is shown for highly co-expressed gene pairs. Solid symbols indicate gene pairs including AP2-G. The number of cells (n) used to evaluate co-expression is shown for each cluster.

nature research

Corresponding author(s): Björn F. C. Kafsack, Ph.D.

☐ Initial submission ☐ Revised version ☒ Final submission

Life Sciences Reporting Summary

Nature Research wishes to improve the reproducibility of the work that we publish. This form is intended for publication with all accepted life science papers and provides structure for consistency and transparency in reporting. Every life science submission will use this form; some list items might not apply to an individual manuscript, but all fields must be completed for clarity.

For further information on the points included in this form, see Reporting Life Sciences Research. For further information on Nature Research policies, including our data availability policy, see Authors & Referees and the Editorial Policy Checklist.

Experimental design

1. Sample size

Describe how sample size was determined.

As these experiments were the first of their kind and sensitivity levels were unknown we opted for the technology that allowed us to sequence the largest number of cells. No statistical methods were used to chose sample size

2. Data exclusions

Describe any data exclusions.

No samples were excluded. Quality filtering of cells is explicitly indicated in the methods. Specifically, cells in which less than 100/300 detected UMIs (ring/late stages) and genes detected in less than 3 cells were excluded from analysis.

3. Replication

Describe whether the experimental findings were reliably reproduced.

Experimental findings were reliably reproduced by technical and biological replicates. scRNA-seq findings in a transgenic parasite line were reliably reproduced in a wildtype parasite line as extensively outlined in the manuscript.

4. Randomization

Describe how samples/organisms/participants were allocated into experimental groups.

Randomization was not performed.

5. Blinding

Describe whether the investigators were blinded to group allocation during data collection and/or analysis.

No blinding was done.

Note: all studies involving animals and/or human research participants must disclose whether blinding and randomization were used.

6. Statistical parameters

For all figures and tables that use statistical methods, confirm that the following items are present in relevant figure legends (or in the Methods section if additional space is needed).

n/a	Confirmed
☐	☒ The exact sample size (*n*) for each experimental group/condition, given as a discrete number and unit of measurement (animals, litters, cultures, etc.)
☐	☒ A description of how samples were collected, noting whether measurements were taken from distinct samples or whether the same sample was measured repeatedly
☐	☒ A statement indicating how many times each experiment was replicated
☐	☒ The statistical test(s) used and whether they are one- or two-sided (note: only common tests should be described solely by name; more complex techniques should be described in the Methods section)
☐	☒ A description of any assumptions or corrections, such as an adjustment for multiple comparisons
☐	☒ The test results (e.g. *P* values) given as exact values whenever possible and with confidence intervals noted
☐	☒ A clear description of statistics including central tendency (e.g. median, mean) and variation (e.g. standard deviation, interquartile range)
☐	☒ Clearly defined error bars

See the web collection on statistics for biologists for further resources and guidance.

Software

Policy information about availability of computer code

7. Software

Describe the software used to analyze the data in this study.	R was used for statistical analyses and single cell analysis including the following R packages: Seurat, Monocle, igraph, ggplot2, rgl Dropseq toolbox (including Picard tools and STAR aligner) FlowJo for analysis of Flow Cytometric Data Cytoscape for network visualization SCANACE for AP2-G motif mapping PANTHER (Protein ANalysis THrough Evolutionary Relationships) for LSD2 functional assignment NCBI Conserved Domain Database for LSD2 functional assignment phylogeny-aware multiple sequence aligner webPRANK for protein sequence alignment ImageJ and ImageJ Deconvolution Lab2 plugin for post-processing of micrographs.

For manuscripts utilizing custom algorithms or software that are central to the paper but not yet described in the published literature, software must be made available to editors and reviewers upon request. We strongly encourage code deposition in a community repository (e.g. GitHub). *Nature Methods* guidance for providing algorithms and software for publication provides further information on this topic.

Materials and reagents

Policy information about availability of materials

8. Materials availability

Indicate whether there are restrictions on availability of unique materials or if these materials are only available for distribution by a for-profit company.	All unique materials used are readily available from the authors or from standard commercial sources

9. Antibodies

Describe the antibodies used and how they were validated for use in the system under study (i.e. assay and species).	No antibodies were used.

10. Eukaryotic cell lines

a. State the source of each eukaryotic cell line used.	NF54 was obtained from MR4. DCJ was obtained from the Deitsch lab and AP2-G-DD was obtained from the Llinas lab.
b. Describe the method of cell line authentication used.	Expected phenotype and drug resistance,. Specifically, DCJ parasites were resistant to Blasticidin-S (Spring 2016). AP2-G-DD parasites were resistant to WR99210 and produced wild-type (NF54) level of gametocytes when cultured in the presence of 0.5 µM Shield1 ligand but not when cultured with solvent control (June 2017). No other methods were used to authenticate cell lines.
c. Report whether the cell lines were tested for mycoplasma contamination.	Cultures were tested semi-annually. Also comparisons were made between treated and untreated cultures of the same line split at the start of an experiment.
d. If any of the cell lines used are listed in the database of commonly misidentified cell lines maintained by ICLAC, provide a scientific rationale for their use.	No commonly misidentified cell lines were used.

Animals and human research participants

Policy information about studies involving animals; when reporting animal research, follow the ARRIVE guidelines

11. Description of research animals

Provide details on animals and/or animal-derived materials used in the study.	No animals were used in this study.

Policy information about studies involving human research participants

12. Description of human research participants

Describe the covariate-relevant population characteristics of the human research participants.	This study did not involve human research participants.